Monthly Notices of the ROYAL ASTRONOMICAL SOCIETY

MNRAS **522,** 466–476 (2023) https://doi.org/10.1093/mnras/stad972
Advance Access publication 2023 March 30

Coalescing black hole binaries from globular clusters: mass distributions and comparison to gravitational wave data from GWTC-3

Fabio Antonini [1]★ Mark Gieles [2,3] Fani Dosopoulou[4,5] and Debatri Chattopadhyay [1]

[1] *Gravity Exploration Institute, School of Physics and Astronomy, Cardiff University, Cardiff CF24 3AA, UK*
[2] *ICREA, Pg. Lluís Companys 23, E08010 Barcelona, Spain*
[3] *Institut de Ciències del Cosmos (ICCUB), Universitat de Barcelona (IEEC-UB), Martí Franquès 1, E08028 Barcelona, Spain*
[4] *Princeton Center for Theoretical Science, Princeton University, Princeton, NJ 08544, USA*
[5] *Department of Astrophysical Sciences, Princeton University, Princeton, NJ 08544, USA*

Accepted 2023 March 24. Received 2023 February 22; in original form 2022 July 19

ABSTRACT

We use our cluster population model, `cBHBd`, to explore the mass distribution of merging black hole binaries formed dynamically in globular clusters. We include in our models the effect of mass growth through hierarchical mergers and compare the resulting distributions to those inferred from the third gravitational wave transient catalogue. We find that none of our models can reproduce the peak at $m_1 \simeq 10\,\mathrm{M}_\odot$ in the primary black hole mass distribution that is inferred from the data. This disfavours a scenario where most of the sources are formed in globular clusters. On the other hand, a globular cluster origin can account for the inferred secondary peak at $m_1 \simeq 35\,\mathrm{M}_\odot$, which requires that the most massive clusters form with half-mass densities $\rho_{\rm h,0} \gtrsim 10^4\ \mathrm{M}_\odot\,\mathrm{pc}^{-3}$. Finally, we find that the lack of a high-mass cut-off in the inferred mass distribution can be explained by the repopulation of an initial mass gap through hierarchical mergers. Matching the inferred merger rate above $\simeq$50 $\mathrm{M}_\odot$ requires both initial cluster densities $\rho_{\rm h,0} \gtrsim 10^4\ \mathrm{M}_\odot\,\mathrm{pc}^{-3}$, and that black holes form with nearly zero spin. A hierarchical merger scenario makes specific predictions for the appearance and position of multiple peaks in the black hole mass distribution, which can be tested against future data.

Key words: stars: kinematics and dynamics – galaxies: star clusters: general – globular clusters: general.

1 INTRODUCTION

The analysis of gravitational wave (GW) observations has identified structures in the mass distribution of the observed population (Tiwari & Fairhurst 2021). Some of these structures already emerged from the analysis of the second gravitational wave transient catalogue (GWTC-2; Abbott 2021; Abbott et al. 2021c). However, thanks to the increased number of events in the new GWTC-3 (Abbott et al. 2021a, b), we are now more confident of their statistical significance. In particular, three important features in the underlining black hole (BH) mass distribution have been uncovered: (i) the distribution of primary BH masses has a strong peak at about $\simeq 10\,\mathrm{M}_\odot$; (ii) there is clear evidence for a secondary peak at $\simeq 35\,\mathrm{M}_\odot$; and (iii) there is no evidence for any mass gap above ≈40–60 $\mathrm{M}_\odot$, which is predicted by stellar evolution models due to pulsational pair-instability and pair-instability in massive stars (e.g. Spera & Mapelli 2017; Woosley 2017; Olejak et al. 2022). In this article, we perform a large number of cluster simulations to understand whether (i), (ii), and (iii) can be explained by a globular cluster (GC) origin for the sources.

The formation of BH binary mergers, including those with components above the upper mass gap, might be explained by several formation pathways. These include binary stellar evolution (e.g. Dominik et al. 2012; Mink & Belczynski 2015; Mandel & De Mink 2016; Farmer et al. 2020; Costa et al. 2021), multiple star interactions (e.g. Antonini, Toonen & Hamers 2017; Silsbee & Tremaine 2017; Fragione, Loeb & Rasio 2020; Hamers et al. 2021; Liu & Lai 2021; Stegmann et al. 2022), stellar collisions in open clusters (e.g. Di Carlo et al. 2020; Kremer et al. 2020; Banerjee 2021a; Dall'Amico et al. 2021; Chattopadhyay et al. 2022), primordial BHs (e.g. Ballesteros, Serpico & Taoso 2018; Gow et al. 2020; De Luca et al. 2021), and formation in active galactic nuclei (e.g. Bartos et al. 2016; Stone, Metzger & Haiman 2016; Yang et al. 2019; Tagawa et al. 2021b). One widely discussed scenario is formation through three body dynamical interactions in dense stellar environments such as nuclear star clusters (e.g. Miller & Lauburg 2009; O'Leary, Kocsis & Loeb 2009; Antonini & Rasio 2016; Antonini, Gieles & Gualandris 2019; Fragione et al. 2022) and GCs (e.g. Kulkarni, Hut & McMillan 1993; Sigurdsson & Hernquist 1993; Banerjee, Baumgardt & Kroupa 2010; Rodriguez et al. 2015; Rodriguez, Chatterjee & Rasio 2016; Askar et al. 2017; Fragione & Kocsis 2018; Chattopadhyay et al. 2022).

The mass distribution of coalescing BH binaries produced in GCs has been investigated in several studies (e.g. Rodriguez et al. 2016; Askar et al. 2017; Park et al. 2017; Antonini & Gieles 2020a; Mapelli et al. 2022; Zevin & Holz 2022). Previous work suggests that GCs are an environment where BH binaries can efficiently assemble and merge, providing one of the main formation channels of BH binary

★ E-mail: antoninif@cardiff.ac.uk

coalescences in the Universe (Portegies Zwart & McMillan 2000). In particular, it has been argued that due to the high escape velocities of GCs, BH mass growth can occur through consecutive mergers, populating any mass gap created by stellar processes (Rodriguez et al. 2018, 2020; Doctor et al. 2020; Kimball et al. 2020, 2021; Tagawa et al. 2021a). In this scenario, a BH that is formed from a previous merger and is retained inside the cluster, sinks back to the cluster core where it dynamically couples with another BH and merges with it after a series of binary-single encounters. If this process repeats multiple times, significant mass growth can occur (Antonini & Rasio 2016; Fishbach, Holz & Farr 2017; Gerosa & Berti 2017). A direct comparison of model predictions with data, however, are rare (Mould, Gerosa & Taylor 2022). It remains therefore an open question whether a GC origin provides a plausible explanation for the inconclusive evidence for an upper mass gap in the GW data, and whether the other features of the inferred BH mass distribution can also be reproduced. A putative successful GC model will then provide useful constraints on the properties of GCs and their BHs at birth.

In this work, we adopt our new fast method for the evolution of star clusters and their binary BHs, `cBHBd` (Antonini & Gieles 2020b), to study the mass distribution of BHs produced dynamically in GCs, including the effect of hierarchical mergers and a novel recipe for sampling masses of the binary BH components and the interlopers. Our efficient approach allows us to address how model assumptions affect the final results, place error bars on merger rate estimates, compare to the distributions inferred from the new GW data catalogue GWTC-3, and, finally, asses a hierarchical merger origin for the formation of the most massive BHs detected by LIGO and Virgo.

In Section 2, we describe our methodology and approximations. In Section 3, we describe our main results, and the importance of model assumptions. We conclude and summarise our results in Section 4.

2 CLUSTER MODELS WITH HIERARCHICAL MERGERS

We simulate the evolution of BH binaries in star clusters using our code `cBHBd`, which we modify in order to include hierarchical mergers. We define here hierarchical mergers as binary mergers in which at least one of the two BH components is a BH remnant that was formed from a previous merger.

Our method is based on Hénon's principle (Hénon 1975), which states that the rate of heat generation in the core is a constant fraction of the total cluster energy per half-mass relaxation time. Thus, the energy production rate in the core, which we assume is produced by BH binaries, is regulated by the energy demand of the entire system (Breen & Heggie 2013). The lifetime and the merger rate of BHs in the cluster can be linked to the evolution of the cluster itself as described in details in Antonini & Gieles (2020b). Then, three ingredients are needed in order to determine the formation of BH binaries, their merger rate, and their properties: (i) a model for the evolution of the cluster global properties; (ii) a model for binary BH dynamics; and (iii) a realistic set of initial BH masses.

We start by sampling the masses of the stellar progenitors of BHs from a standard mass function, $\phi(m_\star) \propto m_\star^{-2.3}$ (Salpeter 1955; Kroupa 2001), with masses in the range 20–130 $M_\odot$. For a given cluster metallicity, Z, we evolve the stars to BHs using the Single Stellar Evolution (`SSE`) package (Hurley, Tout & Pols 2002), which we modified to include updated prescriptions for stellar winds and mass-loss (following Vink, de Koter & Lamers 2001), and for pair-instability in massive stars (following Spera & Mapelli 2017). We therefore evolve the BH progenitors as single stars, assuming a zero binary fraction initially. At the end of this phase, the total number of BHs in a cluster model is calculate by assuming a Kroupa (2001) initial mass function in the mass range 0.1–130 $M_\odot$. The value of the largest BH mass formed in the model depends on metallicity and varies between $\simeq$25 $M_\odot$ for $Z = 2 \times 10^{-2}$ and $\simeq$55 $M_\odot$ for $Z = 1 \times 10^{-4}$. For each BH we compute a natal kick velocity from a Maxwellian distribution with dispersion 265 km s^{-1} (Hobbs et al. 2005), lowered by the amount of mass that falls back into the forming compact object (Fryer et al. 2012). In most of our models, we start the BHs all with the same value of the spin angular momentum, χ, where $\vec{\chi} = \vec{S}/m^2$ is the dimensionless spin of the BH and $\vec{S}$ is the spin angular momentum in units of m^2. In one model, the initial value of χ is sampled from a distribution that is consistent with that inferred from the GW data and is given by the median distribution shown in fig. 15 of Abbott et al. (2021b).

Then, we initialize and evolve the cluster model. The initial conditions are determined by three parameters: the cluster density, $\rho_{\rm h,\,0}$; the cluster mass,M_0; and the total mass in BHs, $M_{\rm BH,\,0}$. The latter is set equal to the total mass in BHs obtained with `SSE`, assuming a Kroupa initial mass function in the range 0.08–130 $M_\odot$ and taking into account that a fraction of the BHs are ejected from the cluster by a natal kick. The time evolution of the cluster properties is then obtained as in Antonini & Gieles (2020a). Briefly, we integrate a set of first order differential equations which determine the time evolution of M , $M_{\rm BH}$, and the cluster half mass radius, $r_{\rm h}$. These models include simple prescriptions for mass-loss and expansion due to stellar evolution and cluster 'evaporation', whereas BHs are assumed to be lost through dynamical ejections.

Finally, we dynamically evolve the BH binaries that form via three-body processes in the cluster core. Our treatment of binary BH formation and evolution follows closely Antonini & Gieles (2020b). The first binary BH forms after the cluster core-collapse time

$$\tau_{\rm cc} = 3.21 t_{\rm rh,0} \tag{1}$$

where $t_{\rm rh,\,0}$ is the initial cluster half-mass relaxation time (for the definition, see equation 10 in Antonini & Gieles 2020b). We assume that the binary is formed with a semimajor axis at the soft-hard boundary, $a_{\rm h} \simeq G\mu/\sigma^2$, with $\mu = m_1\, m_2/(m_1 + m_2)$, where m_1 and m_2 are the masses of the binary components, and $m_1 > m_2$. The expression of $a_{\rm h}$ above is only approximate, and valid under the assumption of equal mass components. Later in Appendix B, we introduce the quantity β and equipartition among BHs of different masses, then the definition is $a_{\rm h} = 0.5\, G m_1\, m_2 \beta$.

The pairing of BHs is done by sampling their masses from the set of BHs still left inside the cluster. We first draw two mass values from the power-law probability distributions $p(m_1) \propto m_1^{\alpha_1}$ and $p(q) = q^{\alpha_2}$, with $\alpha_1 = 8 + 2\alpha$, $\alpha_{\,2} = 3.5 + \alpha$, and $q = m_2/m_1$. Here α is the power law index of the BH mass function, which also evolves with time as the BH population is depleted. The two BH components are then selected by choosing the two BHs that have the mass closest to the values drawn from $p(m_1)$ and $p(q)$ [or $p(m_2)$].

Once selected, the binary is evolved through a sequence of binary-single encounters. Similarly, we find the mass of the third BH interloper from the power-law distribution $p(m_3) \propto m_3^{\alpha_3}$ with $\alpha_3 = \alpha + 1/2$. The adopted expressions for $p(m_1)$, $p(q)$, and $p(m_3)$ are motivated below in Appendix B. The power-law exponent, α, is obtained at the start of the integration for each cluster from a fit to the initial BH mass function after removing BHs that are ejected by natal kicks. The value of α as well as the lower and upper bound of the BH mass function are then recalculated after each time-step. Specifically, the lower bound of the BH mass function is set equal

to the mass of the lightest BH in the cluster, and the upper bound is the mass of the most massive BH. This procedure allows to take into account the evolution of the BH mass function with time due to ejections and the growth of BHs through hierarchical mergers.

Following Samsing (2018), we divide each binary-single encounter in a set of $N_{\rm rs} = 20$ resonant intermediate states and assume that the eccentricity of the binary after each state is sampled from a thermal distribution $N(<e) \propto e^2$. If

$$\sqrt{1-e^2} < h \left(\frac{R_{\rm S}}{a}\right)^{5/14} \tag{2}$$

a merger occurs through a GW capture before the next intermediate binary-single state is formed, where $R_{\rm S} = 2G(m_1 + m_2)/c^2$ and h is a constant of order unity.

If the binary survives the 20 intermediate resonant states, we compute: (i) the new binary semimajor axis, assuming that its binding energy decreases by the fixed fraction $\Delta E/E = 0.2$ (Samsing 2018); (ii) the recoil kick due to energy and angular momentum conservation experienced by the binary centre of mass (Antonini & Rasio 2016)

$$v_{\rm bin}^2 = 0.2G \frac{m_1 m_2}{m_1 + m_2 + m_3} q_3/a \tag{3}$$

with $q_3 = m_3/(m_1 + m_2)$; and (iii) the recoil kick experienced by the interloper:

$$v_3 = v_{\rm bin}/q_3 \, . \tag{4}$$

If $v_{\rm bin} > v_{\rm esc}$, the binary is ejected from the cluster; if $v_3 > v_{\rm esc}$, the interloper is also ejected from the cluster. If the binary is ejected from the cluster, we compute its merger time-scale due to GW energy loss using the standard Peter's formula (Peters 1964).

If $v_{\rm bin} < v_{\rm esc}$, and the binary angular momentum at the end of the triple interaction is such that (Antonini & Gieles 2020b)

$$\sqrt{1-e^2} < 1.3 \left[\frac{G^4 (m_1 m_2)^2 (m_1 + m_2)}{c^5 \dot{E}_{\rm bin}}\right]^{1/7} a^{-5/7} \, , \tag{5}$$

then the BH binary merges before the next binary-single encounter takes place. Binaries that undergo this type of evolution are often named 'in-cluster inspirals' (Rodriguez et al. 2018; Samsing 2018). We then assign the new remnant BH a GW recoil kick, $v_{\rm GW}$, and compute its new spin and mass following Rezzolla et al. (2008). If $v_{\rm GW} > v_{\rm esc}$ the remnant is ejected from the cluster, otherwise we compute the dynamical friction time-scale to sink back to the cluster core

$$\tau_{\rm df} \simeq 1.65 \, r_{\rm in}^2 \frac{\sigma}{\ln \Lambda G m} \tag{6}$$

where (Antonini et al. 2019)

$$r_{\rm in} = r_{\rm h} \sqrt{\frac{v_{\rm esc}^4}{\left(v_{\rm esc}^2 - v_{\rm GW}^2\right)^2} - 1} \tag{7}$$

and only allow the BH to form a new binary after this time. If $v_{\rm bin} < v_{\rm esc}$, but condition equation (5) is not satisfied, then a new interloper is sampled from the given distribution and the binary is evolved through a new binary-single interaction.

Each binary is evolved through a sequence of binary-single encounters until either a merger occurs or it is ejected from the cluster. Then a new binary is formed. The cluster is assumed to live in a state of balanced evolution in which the binary disruption rate is equal to the binary formation rate. Under this assumption, the lifetime of a binary, or the time-scale until a new binary is formed, is simply

$$\tau_{\rm bin} = \frac{m_{\rm ej}}{\dot{M}_{\rm BH}}, \tag{8}$$

where $m_{\rm ej}$ is the total mass ejected by the binary, and $\dot{M}_{\rm BH}$ is the BH mass-loss rate given by the cluster model.

We continue selecting new binaries and evolve them through binary-single encounters until either all BHs have been ejected from the cluster, or until a maximum integration time of $t = 13$ Gyr has passed.

2.1 Cluster initial mass function, formation time, and metallicity

In order to generate predictions for BH binary mergers, we need a GC initial mass function, and a model for how the formation rate and metallicity of clusters evolve with redshift. These ingredients of our models are described below. For this, we follow the approach of Antonini & Gieles (2020a).

The cluster initial mass function is obtained by fitting an evolved Schechter mass function to the observed GC mass function in the Milky Way today (Jordán et al. 2007)

$$\phi_{\rm cl} = A(M + \Delta)^{-2} \exp\left(-\frac{M + \Delta}{M_{\rm c}}\right) \, . \tag{9}$$

This gives the posterior distribution for the parameters $M_{\rm c}$ and Δ. Adopting a simple model for cluster evaporation and mass-loss due to stellar evolution, the corresponding initial GC mass function is given by:

$$\phi_{\rm cl,0} = 2AM_0^{-2} \exp\left(-\frac{M_0}{2M_{\rm c}}\right) . \tag{10}$$

The corresponding fractional mass-loss due to evaporation and stellar evolution is

$$K = \frac{\rho_{\rm GC0}}{\rho_{\rm GC}} = \frac{\int_{M_{\rm lo}}^{\infty} \phi_{\rm cl,0} M_0 {\rm d}M_0}{\int_{M_{\rm lo}}^{\infty} \phi_{\rm cl} M {\rm d}M} = 32.5^{+86.9}_{-17.7} \ (90 \ \text{ per cent cred. intervals}). \tag{11}$$

The spread in K provides an estimate of the uncertainty in the fractional mass-loss from cluster until today, given the 156 Milky Way GC masses. The cluster mass formed per unit volume integrated over all times is (Antonini & Gieles 2020a)

$$\rho_{\rm GC0} = 2.4^{+2.3}_{-1.2} \times 10^{16} \ {\rm M}_\odot \ {\rm Gpc}^{-3} \ (90 \ \text{ per cent cred. intervals}). \tag{12}$$

The large error bars here imply that $\rho_{\rm GC0}$ is uncertain by a factor of $\simeq 2$. In the next sections, we include this uncertainty as well as the uncertainty on K in the predictions for the merger rate.

We obtain the distribution of cluster formation times from the semi-analytical galaxy formation model of El-Badry et al. (2019). The resulting cluster formation history peaks at a redshift of $\sim$4, which is earlier than the peak in the cosmic star formation history (redshift $\sim$2, Madau & Dickinson 2014). We sample the formation redshift of our cluster models from the total cosmic cluster formation rate given by the fiducial model of El-Badry et al. (2019) and integrated over all halo masses. This corresponds to the formation rate per comoving volume of their fig. 8 with their parameters $\beta_\Gamma = 1$ and $\beta_\eta = 1/3$, where β_Γ sets the dependence of the cluster formation efficiency on surface density, and β_η the dependence of the star formation rate on the halo virial mass. Here, we renormalize the cluster formation rate, $\phi_z(z)$, such that $\int_\infty^0 \phi_z {\rm d}z = 1$. Thus, we only sample the cluster formation time from El-Badry et al. (2019), and then rescale the cluster formation rate such to reproduce the total mass density given by our equation (12). We note that the cluster formation model has a negligible impact on the local merger rate and properties of the merging binaries. In Antonini & Gieles (2020a),

we showed that unrealistic models where all clusters are assumed to form at the same time (e.g. $z = 3$) produce similar results than models in which the cluster formation rate is varied with redshift.

For the cluster metallicity, we fit a quadratic polynomial to the observed age–metallicity relation for the Milky Way GCs (VandenBerg et al. 2013) to obtain the mean metallicity

$$\log(Z_{\rm mean}/Z_\odot) \simeq 0.42 + 0.046\left(\frac{t}{\rm Gyr}\right) - 0.017\left(\frac{t}{\rm Gyr}\right)^2. \quad (13)$$

Given the cluster formation redshift, we then assume a log-normal distribution of metallicity around the mean

$$\phi_Z = \frac{\log(e)}{\sqrt{2\pi\sigma^2}}\exp\left\{-\frac{[\log(Z/Z_\odot) - Z_{\rm mean}]^2}{2\sigma^2}\right\}, \quad (14)$$

with standard deviation $\sigma = 0.25$ dex. This takes into account the large spread found in the observed age–metallicity relation for the Milky Way GCs.

2.2 Merger rates and their error bars

Finally, we construct a library of cluster models over a three-dimensional grid of formation time, metallicity, and cluster mass.

We sample the cluster formation redshift over the range $z \in [10; 0]$ with step-size $\Delta z = 0.5$; at a given redshift, the metallicity of the cluster is sampled in the range $Z \in [10^{-4}; 0.02]$ with logarithmic step size $\Delta\log Z = 0.1$; finally, for a given formation time and metallicity, the initial mass of the cluster is varied in the range $M_0 \in [10^2; 2 \times 10^7]$ $\rm M_\odot$, with step size $\Delta\log M_0/M_\odot = 0.1$. The merger rate is then calculated over the grid of cluster models as:

$$\mathcal{R}(\tau) = K\,\rho_{\rm GC}\frac{\sum_z\sum_Z\sum_{M_0}\dot{\mathcal{N}}(\tau; z, Z, M_0)\phi_z\phi_Z\phi_{{\rm cl},0}M_0}{\sum_z\phi_z\sum_Z\phi_Z\sum_{M_0}\phi_{{\rm cl},0}M_0^2}, \quad (15)$$

where $\dot{\mathcal{N}}(\tau; M_0, r_{\rm h,0}, Z)$ is the BH binary merger rate at a look-back time τ corresponding to a cluster with an initial mass M_0, metallicity Z and that formed at a redshift z.

In order to take into account the uncertainties in the initial cluster mass function, we sample 100 values over the posterior distributions of the parameters $M_{\rm c}$ and Δ obtained from the MCMC fit to the Milky Way GC mass function. We also take into account the uncertainty on the mass density of GCs in the Universe, $\rho_{\rm GC}$. We assume that the parameter $\rho_{\rm GC}$ follows a Gaussian distribution with mean $7.3 \times 10^{14}\,\rm M_\odot\,Gpc^{-3}$ and dispersion $\sigma = 2.6 \times 10^{14}\,\rm M_\odot\,Gpc^{-3}$. We sample 100 values from this Gaussian distribution and for each of them we use equation (15) to determine a merger rate estimate for each of the $[M_{\rm c}, \Delta]$ values, and thus obtain a *distribution* of merger rate density values. Since in this work we are interested in the mass distribution of local BH binary mergers, we consider the differential merger rate in the local universe $\rm d\mathcal{R}(z = 0)/dm_1$ and $\rm d\mathcal{R}(z = 0)/dq$, which we compare to the distributions inferred from GWTC-3.

3 RESULTS

3.1 Primary BH mass and mass-ratio distributions

In Antonini & Gieles (2020a), we found good agreement between model predictions and the inferred distribution of primary BH masses within the range of values $m_1 = 15$–40 $\rm M_\odot$. Outside this range, the binary BH merger rate was found to be several orders of magnitude smaller than inferred. The first question we address here is whether the inclusion of hierarchical mergers can reduce the discrepancy at $m_1 \gtrsim 40\,\rm M_\odot$ between models and the inferred astrophysical distributions.

In Fig. 1, we plot the distributions of m_1 and q for three different assumptions about the initial BH mass function. In the upper panels, we use the delayed supernova mechanism, in the middle panels the rapid supernova mechanism (Fryer et al. 2012), and in the lower panels we use the BH mass distribution from Belczynski et al. (2008). These prescriptions produce somewhat different initial BH mass functions, and lead also to different natal kick values. In these models, all clusters are initialized with the same half-mass radius density of $\rho_{\rm h,0} = 10^5\,\rm M_\odot\,pc^{-3}$ and the BHs are all started with zero dimensionless spin parameter, $\chi = 0$.

In the left-hand panel of Fig. 1, we see that the new models produce mergers above the $\sim$50 $\rm M_\odot$ threshold. These mergers are produced by BHs that grow hierarchically through mergers – the vast majority of them are mergers between a first generation BH and a second generation BH. When we include these mergers in our calculation, we find good agreement between the models and the inferred distributions at $m_1 \gtrsim 50$ $\rm M_\odot$, in the sense that the models give a merger rate that is comparable with the inferred value. However, we also note that a simple power-law profile above this mass threshold is not a good representation of the model distributions. Above $m_1 \simeq 50\,\rm M_\odot$, the model distributions are characterised by several peaks. Such higher mass peaks are related to peaks in the BH mass distribution at lower masses. From Fig. 1, we see that the merger rate between first generation BHs peaks at $\simeq$30 and 40 $\rm M_\odot$. Thus, mergers between first and second generation BHs lead to additional peaks at $\simeq (30 + 30)\,\rm M_\odot = 60\,M_\odot$, $(30 + 40)\,\rm M_\odot = 70\,M_\odot$, and $(40 + 40)\,\rm M_\odot = 80\,M_\odot$. The presence of peaks within the pair-instability mass gap and their relation to lower mass peaks in the BH mass distribution is a clear prediction of a hierarchical merger model for the origin of the binaries.

The black histograms in the left-hand panel of Fig. 1 show the results from models in which any remnant BH formed from a previous merger is ejected from the cluster 'by hand'. In these models, the distributions are sharply truncated at $\sim$50 $\rm M_\odot$ since BHs cannot grow hierarchically above this mass value. The merger rate at $m_1 \simeq 10\,\rm M_\odot$ derived from all models is about two orders of magnitude smaller than the inferred rate. This lower-mass peak can be explained, however, through other scenarios, including formation in the galactic field (e.g. Broekgaarden et al. 2022; van Son et al. 2022) and formation in young and open star clusters because of their higher metallicity (e.g. Banerjee 2021b; Chattopadhyay et al. 2022). On the other hand, our models reproduce the inferred merger rate near $m_1 \simeq 30$ $\rm M_\odot$, which can therefore be explained by a GC origin. This peak in the mass distribution is due to mergers involving first-generation BHs, and it is not related to hierarchical mergers.

By comparing the results in Fig. 1 with the models in Antonini & Gieles (2020a), we find that the latter generated a merger rate at $m_1 \lesssim 20$ $\rm M_\odot$ higher by a factor $\lesssim 2$. The reason for this difference is due to the adopted new recipe for sampling the black hole binary components and the interloper masses. In Antonini & Gieles (2020a), we had assumed that $m_1 = m_2 = m_3 = m_{\rm max}$, where $m_{\rm max}$ is the mass of the most massive BH in the cluster. The distributions in Appendix B mean instead that in the current models $\langle m_3\rangle \ll \langle m_1\rangle \simeq \langle m_2\rangle$. Thus, each binary ejects more low-mass BH interloopers lowering the overall BH merger rate at low masses.

In the right-hand panel of Fig. 1, we consider the distribution of the mass-ratio q. The new models result in a significantly higher rate of merging binaries with small mass-ratio, $q \lesssim 0.5$, providing a better match to the inferred distribution than models without hierarchical

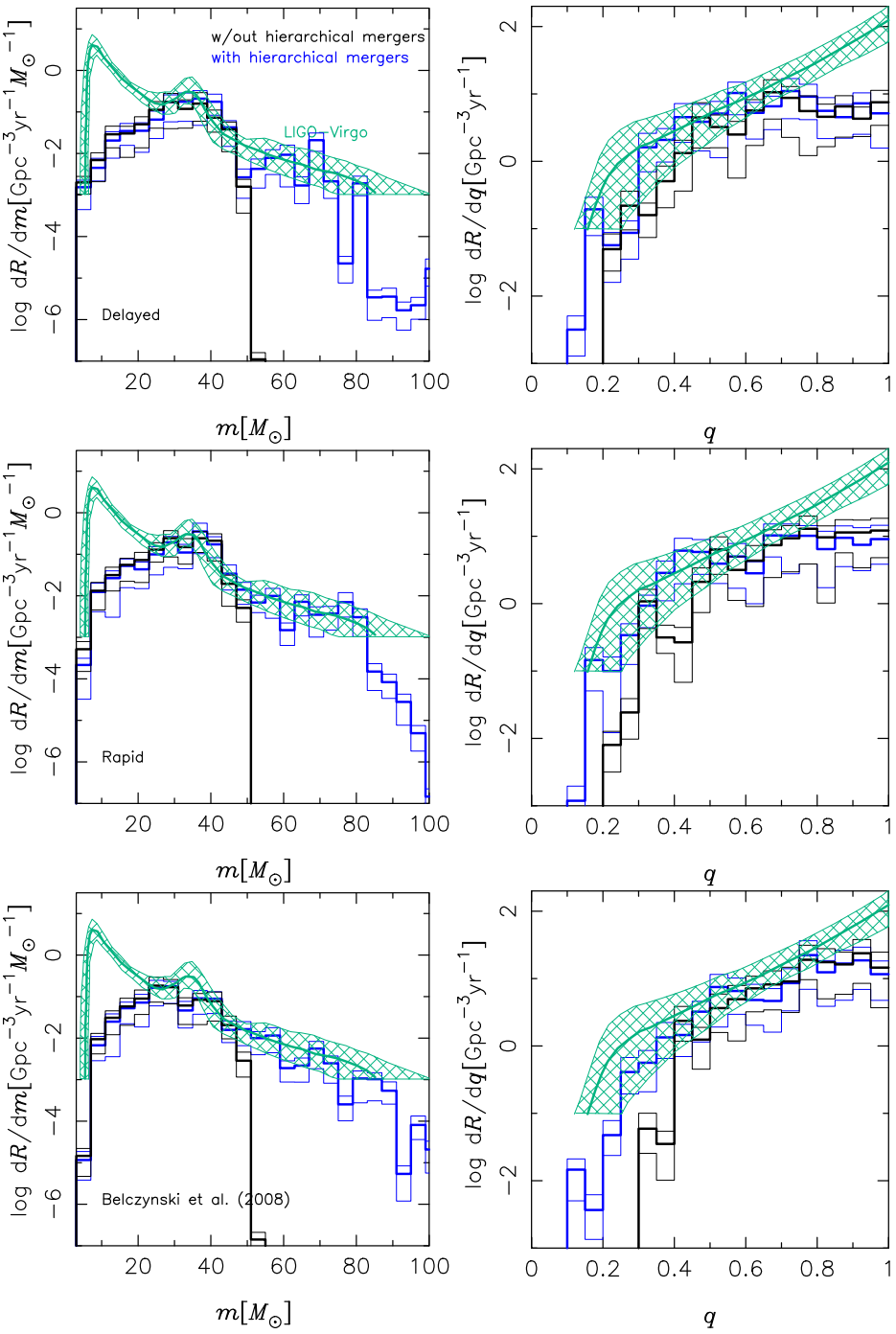

Figure 1. Local distributions of primary BH mass and mass-ratio for merging BH binaries in our best-case scenario where clusters start with high densities, $\rho_{h,0} = 10^5$ M$_\odot$ pc^{-3}, and the BHs are all initialized with zero dimensionless spin parameter $\chi = 0$. Top, middle, and bottom panels correspond to the delayed supernova mechanism, the rapid supernova mechanism, and the BH mass distribution of Belczynski et al. (2008), respectively. Black lines show the corresponding distributions when hierarchical mergers are not included in the calculation, i.e. it is assumed that a BH formed from a previous merger is always ejected from the cluster. Thick lines show median values of the merger rate value, and thin lines the corresponding 90 per cent confidence intervals. The green lines and hatched regions show the median and corresponding 90 per cent confidence regions inferred from the GWTC-3 (Abbott et al. 2021a).

mergers. Most of these additional low-q systems are mergers between a first generation BH and a BH that formed through a previous merger above the pair-instability mass limit. At high values of q, instead, both models with and without hierarchical mergers produce a similar merger rate, which, at $q \gtrsim 0.8$, is about one-order of magnitude smaller than inferred from the data.

In Fig. 2, we show the differential contribution to the local merger rate with respect to the initial cluster mass. This allows us to identify in which type of clusters most of the mergers are formed. The contribution to the total merger rate is nearly constant in log bins between $M_0 = 5 \times 10^4$ M$_\odot$ and 5×10^6 M$_\odot$, whereas it decrease exponentially above this range because of the truncation of the initial

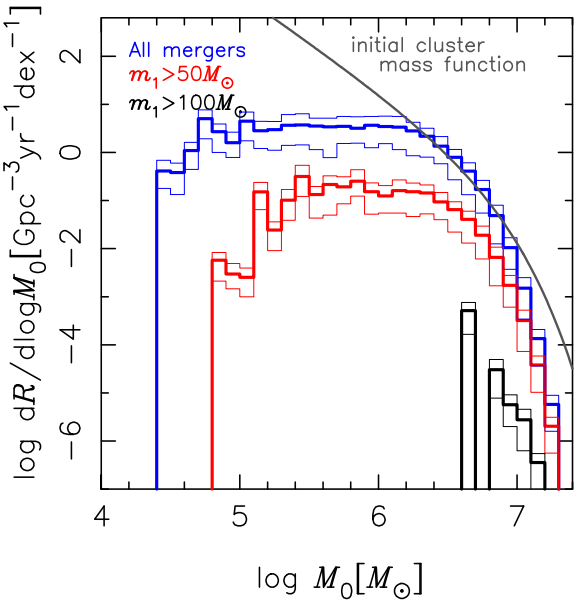

Figure 2. Differential local merger rate as a function of the initial cluster mass. We also show the initial cluster mass function (in arbitrary units) for our best fit value of Schechter mass, log $M_c/M_\odot = 6.26$. The delayed supernova mechanism has been adopted here.

GC mass function at log $M_c/M_\odot \simeq 6.26$. We then show the same cluster mass distribution, but only considering mergers with $m_1 \geq 50$ $M_\odot$ (red histogram). These mergers, involving a primary BH above the mass gap limit, are mostly produced in clusters with relatively large masses, between $\sim 2 \times 10^5$ and 5×10^6 $M_\odot$. The fraction of these higher mass mergers to the total number of mergers in each cluster mass bin increases with cluster mass. By comparing the blue and the red histograms in the figure, we see that at $M_0 \sim 10^7$ $M_\odot$, between 10 per cent and 30 per cent of mergers have a primary with $m_1 > 50$ $M_\odot$. The percentage goes down to ~ 1 per cent in clusters with an initial mass lower than $\simeq 10^6$ $M_\odot$. Finally, we show the M_0 distributions for the most massive mergers produced in our models, $m_1 \geq 100$ $M_\odot$. These BHs originate from at least two previous mergers since their mass is larger than twice the initial mass cut-off at $\simeq 50$ $M_\odot$. These systems are formed in the most massive GCs, with initial mass well above the Schechter mass.

Based on the models of Fig. 2, we compute a local binary BH merger rate of $4.1^{+2.2}_{-2.5}$Gpc^{-3} yr^{-1} (delayed), $4.5^{+2.7}_{-2.9}$Gpc^{-3} yr^{-1} (rapid), and $6.0^{+3.6}_{-4.0}$Gpc^{-3} yr^{-1} (BH mass distribution from Belczynski et al. 2008), at 90 per cent confidence. The binary BH merger rate inferred from the gravitational wave data is estimated to be between 17.9 and 44Gpc^{-3} yr^{-1} (Abbott et al. 2021a), and it is therefore a factor of $\simeq$2–20 larger than the rate computed from our models.

3.2 Effect of initial cluster density, initial spins, and other model variations

The number of heavier BHs produced by a cluster through hierarchical mergers is affected by both the cluster density and the initial spin of the BHs. A larger cluster density means a larger merger rate and escape velocity, and therefore a larger probability that a remnant BH is retained inside the cluster following a recoil kick. Similarly, if the BHs have negligible spins, this translates into a smaller recoil velocity and higher retention probability. Although in the previous section, we have looked at a somewhat optimistic scenario in which clusters all form with high densities and the BHs have initially zero spins, in this section we vary these assumptions and investigate their effect on the BH binary merger rate and properties. We adopt here the delayed supernova mechanism, but similar results are obtained with the rapid supernova prescription and the Belczynski et al. (2008) mass distribution.

In the upper panels of Fig. 3, we vary the initial cluster half-mass density within the range $\rho_{\rm h,\,0} = 10^2$ to 10^5 $M_\odot$ pc^{-3}, and assume that the BHs have zero spins initially. The results illustrate that although our models can in principle account for most mergers above $m_1 \gtrsim 20\,M_\odot$, this is only true under some specific conditions. As we lower the initial cluster half-mass density the merger rate goes down significantly at all values of mass and mass-ratio. The depletion is more significant at masses above the cut-off mass of 50 $M_\odot$ and for $q \lesssim 0.5$. Thus, a scenario where most merging BH binaries with $m_1 \gtrsim 20\,M_\odot$ form in GCs would imply a typical initial cluster density $\rho_0 \gtrsim 10^4$ $M_\odot$ pc^{-3}. It is important to note that this condition would however only apply to clusters with initial mass $M_0 \gtrsim 5 \times 10^4$ $M_\odot$, where most of the merging binaries are formed (see Fig. 2).

In the lower panels of Fig. 3, we show how the results change with changing the initial BH spins. In these models, we keep the initial density to the fixed value $\rho_0 = 10^5$ $M_\odot$ pc^{-3}. We see that the merger rate density distributions are not affected significantly for $m_1 \lesssim 50$ $M_\odot$ and $q \gtrsim 0.5$. This is because the majority of these binaries are made of first generation BHs. Hence, their merger rate is not affected by the recoil kick velocity and by the initial choice of BH spin. On the other hand, the number of BHs formed via hierarchical mergers decreases significantly when higher initial spins are used due to the larger recoil kicks. This leads to a lower merger rate at $m_1 \gtrsim 50$ $M_\odot$ when χ is increased. Even relatively modest initial spins, $\chi = 0.1$, lead to a distribution that does no longer match the inferred distribution. The constrains on χ seems therefore quite strong as a hierarchical origin for all mergers with $m_1 \gtrsim 50$ $M_\odot$ would require that BHs are formed with nearly zero spin.

Finally, we consider six additional model realisations. In one model, we assume that the BHs receive no kick at formation and that the initial density is the same for all clusters, $\rho_{\rm h,0} = 10^5$ $M_\odot$ pc^{-3}. In another model, we assume that the cluster half-mass radius scales as

$$\log\left(\frac{r_{\rm h,0}}{\rm pc}\right) = -3.56 + 0.615\log\left(\frac{M_0}{M_\odot}\right)\,. \qquad (16)$$

This latter relation was derived by Gieles et al. (2010) from the results of Haşegan et al. (2005) who fit this Faber–Jackson-like relation to ultra-compact dwarf galaxies and elliptical galaxies. Gieles et al. (2010) derived the initial mass–radius relation correcting for mass-loss and expansion by stellar evolution and correcting radii for projection. We consider an additional model realisation where we did not include any prescription for pair instability so that the initial BH mass function has no upper gap and BHs can form above 50 $M_\odot$. Moreover, we consider two models where the initial mass function above 0.5 $M_\odot$ is assumed to scale as $\phi(m_\star) \propto m_\star^{-2}$ (top-heavy) and $\phi(m_\star) \propto m_\star^{-2.6}$ (bottom heavy), respectively. Finally, we evolve two additional models where our standard Wolf–Rayet winds based on Hamann & Koesterke (1998) and Vink & de Koter (2005) are multiplied by a factor $f_{\rm WR} = 0.1$ and $f_{\rm WR} = 5$ (e.g. Broekgaarden et al. 2022). Unless otherwise specified, all the other model parameters are the same as before, i.e. delayed supernova mechanism, $\chi = 0$, fallback kicks, etc.

Fig. 4 shows that the mass properties of the BH binaries produced in the new models without birth kicks and with the new $r_{\rm h}$–M relation are similar to those found previously in Section 3.1. The fact that adopting the mass-radius relation equation (16) does not change

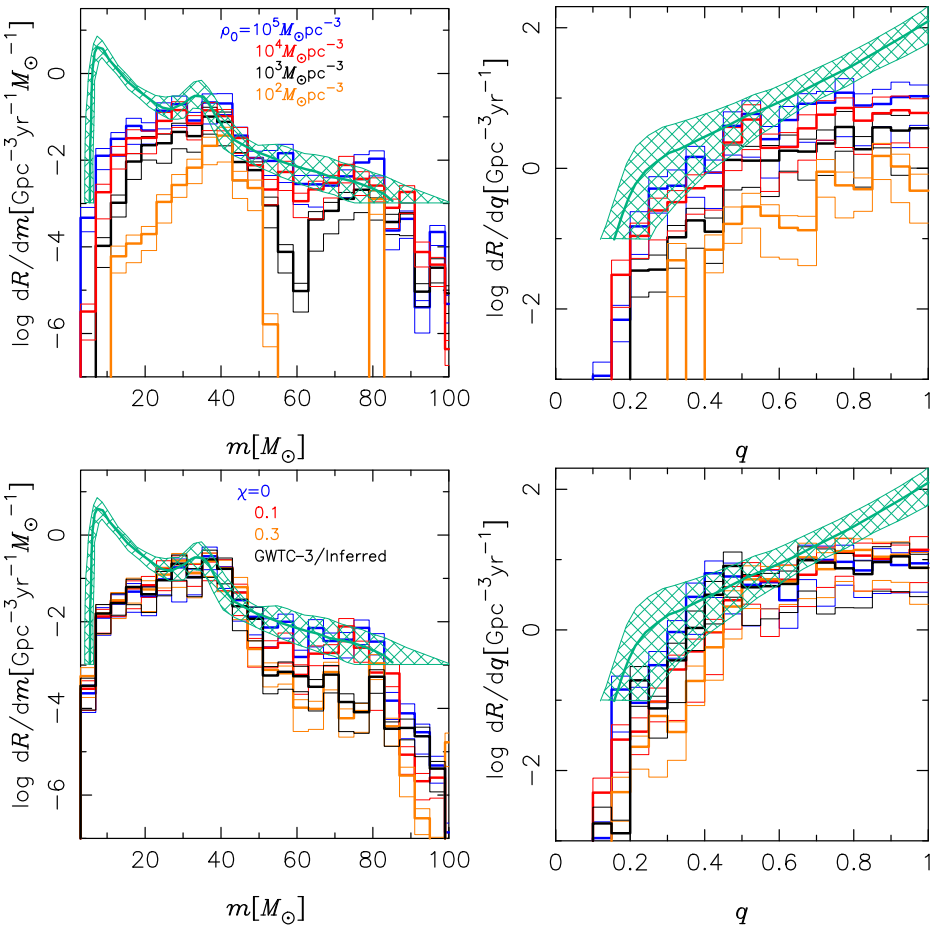

Figure 3. Dependence of mass and mass-ratio distributions on initial cluster half-mass density, and initial BH spins. The delayed supernova model is assumed here. Top panels use $\chi = 0$ and the half-mass density of the cluster is varied as indicated. In the bottom panel we take $\rho_{h,0} = 10^5$ M$_\odot$ pc^{-3} and change the initial value of χ; the black histograms show the results for a model where the initial value of χ is sampled using the inferred distribution of BH spins shown in fig. 15 of Abbott et al. (2021b). In all the other models, the BHs all form with the same value of χ as indicated.

significantly our results is not surprising. Clusters with an initial mass $M_0 \sim 10^6$ M$_\odot$ contribute the most to the merger rate (see Fig. 2). The initial half-mass density of these clusters as derived from equation (16) is $\rho_{h,0} \simeq 5 \times 10^4$ M$_\odot$ pc^{-3}. This is comparable with the constant density value of 10^5 M$_\odot$ pc^{-3} adopted previously. Interestingly, the results of models with no birth kicks show that assuming zero velocity kicks at birth increases slightly the merger rate at the lower mass end of the m_1 distribution and the number of merging binaries with asymmetric masses. On the other hand, the shape and normalisation of the distributions at masses higher than $m_1 \gtrsim 20$ M$_\odot$ remain virtually the same as in the fallback kick model.

The model without pair instability physics leads to a mass distribution which is significantly different from the other model realisations, showing how our results can depend on the assumptions about stellar evolution and the adopted prescriptions. In this case, the mass distribution still peaks at $m_1 \sim 30$ M$_\odot$, whereas the other peak near 40 M$_\odot$ is no longer present. A secondary peak is found near 70 M$_\odot$. For masses larger than this value, the merger rate drops and becomes much smaller than the rate inferred from the GW data.

In the model with a top-heavy stellar mass function, the overall merger rate is higher than for our standard models due to the larger number of BHs formed. On the other hand, for a bottom-heavy mass function the total merger rate is significantly reduced due to the fewer massive stars formed. Our model with modified Wolf–Rayet wind mass-loss rate lead to results that are qualitatively similar to those obtained under our more standard assumptions.

That our resulting mass distributions are sensitive to the initial BH mass function, and therefore to the uncertain stellar evolution prescriptions is expected. It is interesting, however, that most of our models share similar properties. Specifically: (i) the inferred peak in the merger rate at 10 M$_\odot$ is much lower than the one inferred from the data, and (ii) the distribution of m_1 presents a main peak at near 35 M$_\odot$. The main reason why there are so few mergers with small masses is because of the relatively low number of light BHs in the initial mass function. This is due to the low metallicity of GCs, which results in low wind mass-loss and large BH masses. The other reason why the mass distribution of merging binaries peaks at relatively high values is dynamics. The masses of the binary components tend to be sampled near the top end of the BH mass function, due to the high value of the power law exponents that appear in the density probability functions p_1 and p_2 (see Section B). On the other hand, the flatter p_3 distribution means that the ejected BH interlopers will be on average lighter than the binary BH components. These lighter BHs are therefore no longer available for merging.

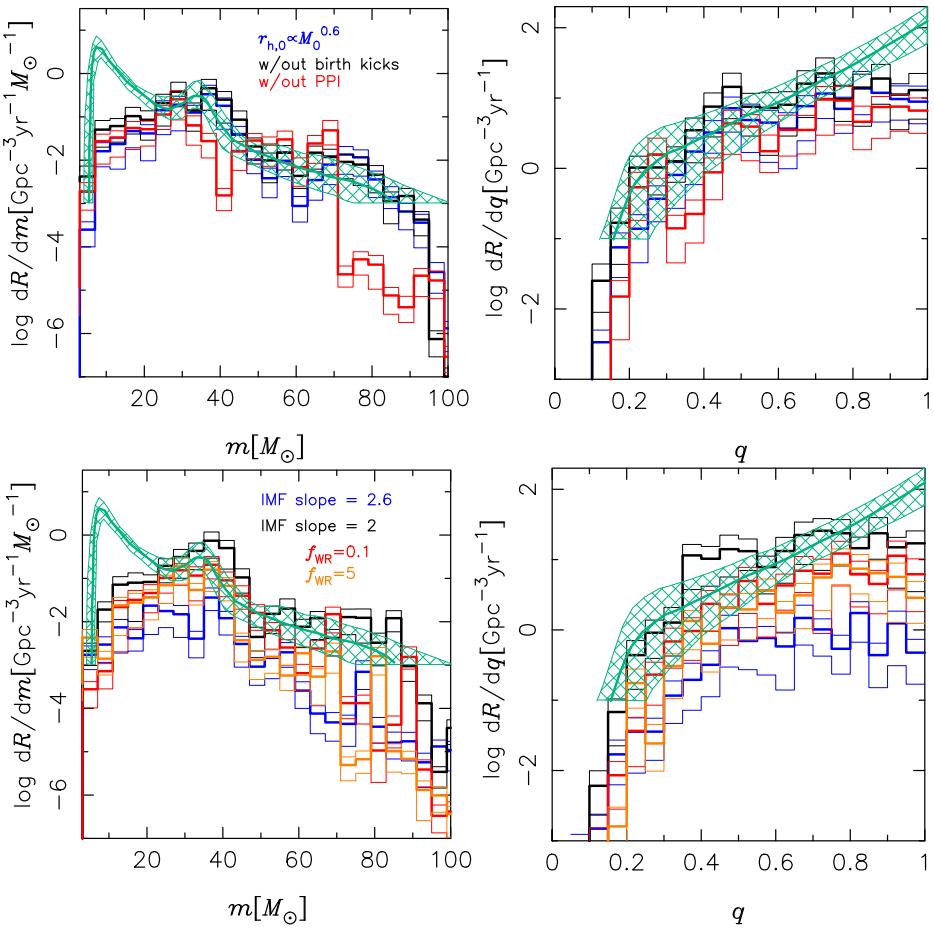

Figure 4. Results for six alternative models. Left-hand panel: blue histograms are for a model in which the initial cluster half-mass radius is assumed to scale with cluster mass as in equation (16); the blue histograms correspond to a model in which the BH birth kicks are zero; the red histograms correspond to a model where the recipes for pulsation pair instability were switched off. Right-hand panel: blue and black histograms are the results obtained assuming that the initial stellar mass function for massive stars scales as $\phi(m_\star) \propto m_\star^{-2}$ and $\phi(m_\star) \propto m_\star^{-2.6}$, respectively. In the red and orange histograms we have multiplied our standard wind mass-loss rate on the Wolf–Rayet stage by a factor $f_{\rm WR} = 0.1$ and $f_{\rm WR} = 5$. We have used the delayed supernova mechanism, and, unless otherwise specified, all the other model parameters are the same as in Fig. 1.

4 CONCLUSIONS

In this work we have used our fast cluster evolution code, cBHBd, to investigate the mass distribution of BH binaries produced dynamically in dense GCs. We compared our results with the astrophysical distribution of BH binary masses inferred from GWTC-3 to make inference about the astrophysical origin of the sources. For the first time, we have included hierarchical mergers in our models. This allowed us to address the question of whether a dynamical formation scenario is a feasible explanation for the detected BHs within the so called 'upper mass gap'. Such a mass gap in the initial BH mass function is predicted by stellar evolution theories, and in our models is located at $\gtrsim$50 M$_\odot$. Because cBHBd is highly efficient compared wtih other techniques (e.g. Monte Carlo, *N*-body), we were able to systematically investigate the impact of model assumptions on or results. Our main conclusions are summarised below:

(i) A purely GC formation scenario for the BH binaries detected by LIGO and Virgo is inconsistent with the $\simeq$ 10 M$_\odot$ peak in the primary BH mass distribution that is inferred from the data. This likely excludes a scenario where the majority of the sources were formed in GCs.

(ii) A GC origin can easily account for the secondary mass peak at $m_1 \simeq 35$ M$_\odot$ inferred from the data. This requires that clusters form with initial half-mass density $\gtrsim 10^4$ M$_\odot$ pc^{-3}. Assumptions about the initial BH spins and the supernova mechanism have no effect on this conclusion.

(iii) Dynamical formation in GCs can explain the inferred merger rate of all BH binaries with $m_1 \gtrsim 20$ M$_\odot$ and $q \lesssim 0.8$, including binaries with component masses lying above the assumed mass limit due to pair-instability. For this to be true we require that both the most massive GCs, $M_0 \gtrsim 10^5$ M$_\odot$, form with half-mass density $\gtrsim 10^4$ M$_\odot$ pc^{-3}, and that the birth spins of BHs are nearly zero. Even small deviations from this latter condition lead to a merger rate above 50 M$_\odot$ that is orders of magnitude smaller than the inferred rate.

(iv) A hierarchical merger scenario predicts the appearance of multiple peaks in the primary BH mass distribution and within the upper mass gap due to a pile-up of mergers between first and second generation BHs. Intergeneration mergers lead to a simple relation between the mass value of any of such peaks and that of peaks found at masses lower than the pair-instability limit. These features can be tested against future GW data to place constrains on a GC origin for the sources.

Additional constraints on the formation of BH mergers can be placed by exploring correlations between binary parameters, which we have not considered here, but plan to study in a future work. For example, a BH formed from a previous merger will have a spin $\chi \simeq 0.7$. We expect therefore a change in the value of the typical effective and precession spin parameters of binaries with components within the upper mass gap (e.g. Baibhav et al. 2020; Tagawa et al. 2021a) and an increase in spin magnitude for systems with more unequal mass-ratio. Binaries formed dynamically will also have larger eccentricities, which can lead to a positive correlation between eccentricity, spin and binary mass in the overall population. The analysis of the data from GWTC-3 has shown marginal evidence that the spin distribution broadens above 30 $M_\odot$, and that the mass-ratio and spin are correlated in the sense that spins are larger for more asymmetric binaries (Abbott et al. 2021a). The evidence for these correlations remain weak, but it suggests that future analysis based on larger data sets will soon be able to provide more stringent constrains. The residual eccentricity of a binary is by itself another potentially powerful tool for identifying sources formed in clusters. Romero-Shaw, Lasky & Thrane (2022) suggest that a significant fraction of the detected GW sources in GWTC-3 show support for eccentricity $\gtrsim$0.1 at 10Hz. Their results indicate that densely populated star clusters may produce the majority of the observed mergers.

Finally, it is worth noting that in our work we used the pair-instability prescriptions from Spera & Mapelli (2017). This gives an upper limit in the initial BH mass function of about 50 $M_\odot$. However, there are several uncertainties in the modelling, and different assumptions can lead to significantly different values for the high-mass cut-off, generally in the range 40–70 $M_\odot$ (Giacobbo, Mapelli & Spera 2018; Farmer et al. 2020; Costa et al. 2021; Fryer, Olejak & Belczynski 2022). Exploring the effect of these uncertainties is beyond the scope of this paper, but should be considered in future work.

ACKNOWLEDGEMENTS

Some of the processing of the results has been done using the PYTHON programming language and the following open source modules: NUMPY. [1], SCIPY [2], MATPLOTLIB.[3] We acknowledge the support of the Supercomputing Wales project, which is part-funded by the European Regional Development Fund (ERDF) via Welsh Government. FA acknowledges support from a Rutherford fellowship (ST/P00492X/1) from the Science and Technology Facilities Council. MG acknowledges support from the Ministry of Science and Innovation (EUR2020-112157, PID2021-125485NB-C22, and CEX2019-000918-M funded by MCIN/AEI/10.13039/501100011033) and from AGAUR (SGR-2021-01069).

DATA AVAILABILITY

The data underlying this article will be shared on a reasonable request to the corresponding author.

REFERENCES

Abbott R. E. A. , 2021, GWTC-2: Compact Binary Coalescences Observed by LIGO and Virgo during the First Half of the Third Observing Run, Physical Review X, 11, 021053

[1]http://www.numpy.org.
[2]http://www.scipy.org.
[3]http://matplotlib.sourceforge.net.

Abbott R., et al., 2021a, preprint (arXiv:2111.03606)
Abbott R., et al., 2021b, preprint (arXiv:2111.03634)
Abbott R., et al., 2021c, ApJ, 913, L7
Antonini F., Gieles M., 2020a, Phys. Rev. D, 102, 123016
Antonini F., Gieles M., 2020b, MNRAS, 492, 2936
Antonini F., Rasio F. A., 2016, ApJ, 831, 187
Antonini F., Toonen S., Hamers A. S., 2017, ApJ, 841, 77
Antonini F., Gieles M., Gualandris A., 2019, MNRAS, 486, 5008
Askar A., Szkudlarek M., Gondek-Rosińska D., Giersz M., Bulik T., 2017, MNRAS, 464, L36
Baibhav V., Gerosa D., Berti E., Wong K. W. K., Helfer T., Mould M., 2020, Phys. Rev. D, 102, 043002
Ballesteros G., Serpico P. D., Taoso M., 2018, J. Cosmology Astropart. Phys., 2018, 043
Banerjee S., 2021a, MNRAS, 500, 3002
Banerjee S., 2021b, MNRAS, 503, 3371
Banerjee S., Baumgardt H., Kroupa P., 2010, MNRAS, 402, 371
Bartos I. , Kocsis B. , Haiman Z. , Márka S. , 2017, ApJ, 835, 165
Belczynski K., Kalogera V., Rasio F. A., Taam R. E., Zezas A., Bulik T., Maccarone T. J., Ivanova N., 2008, ApJS, 174, 223
Breen P. G., Heggie D. C., 2013, MNRAS, 432, 2779
Broekgaarden F. S. et al., 2022, MNRAS, 516, 5737–5761
Chattopadhyay D., Hurley J., Stevenson S., Raidani A., 2022, MNRAS, 513, 4527
Costa G., Bressan A., Mapelli M., Marigo P., Iorio G., Spera M., 2021, MNRAS, 501, 4514
Dall'Amico M., Mapelli M., Di Carlo U. N., Bouffanais Y., Rastello S., Santoliquido F., Ballone A., Arca Sedda M., 2021, MNRAS, 508, 3045
De Luca V., Desjacques V., Franciolini G., Pani P., Riotto A., 2021, Phys. Rev. Lett., 126, 051101
Di Carlo U. N., Mapelli M., Bouffanais Y., Giacobbo N., Santoliquido F., Bressan A., Spera M., Haardt F., 2020, MNRAS, 497, 1043
Doctor Z., Wysocki D., O'Shaughnessy R., Holz D. E., Farr B., 2020, ApJ, 893, 35
Dominik M. , Belczynski K. , Fryer C. , Holz D. E. , Berti E. , Bulik T. , Mandel I. , O'Shaughnessy R. , 2012, Double compact objects. I. The significance of the common envelope on merger rates, ApJ, 759, 52, http://adslabs.org/adsabs/abs/2012ApJ...759...52D/
El-Badry K., Quataert E., Weisz D. R., Choksi N., Boylan-Kolchin M., 2019, MNRAS, 482, 4528
Farmer R., Renzo M., de Mink S. E., Fishbach M., Justham S., 2020, ApJ, 902, L36
Fishbach M., Holz D. E., Farr B., 2017, ApJ, 840, L24
Fragione G., Kocsis B., 2018, Phys. Rev. Lett., 121, 161103
Fragione G., Loeb A., Rasio F. A., 2020, ApJ, 895, L15
Fragione G. , Loeb A. , Kocsis B. , Rasio F. A. , 2022, ApJ, 933, 9
Fryer C. L., Belczynski K., Wiktorowicz G., Dominik M., Kalogera V., Holz D. E., 2012, ApJ, 749, 91
Fryer C. L., Olejak A., Belczynski K., 2022, ApJ, 931, 94
Gerosa D., Berti E., 2017, Phys. Rev. D, 95, 124046
Giacobbo N., Mapelli M., Spera M., 2018, MNRAS, 474, 2959
Gieles M., Baumgardt H., Heggie D. C., Lamers H. J. G. L. M., 2010, MNRAS, 408, L16
Gow A. D., Byrnes C. T., Hall A., Peacock J. A., 2020, J. Cosmology Astropart. Phys., 2020, 031
Hamann W. R., Koesterke L., 1998, A&A, 335, 1003
Hamers A. S., Fragione G., Neunteufel P., Kocsis B., 2021, MNRAS, 506, 5345
Haşegan M. et al., 2005, ApJ, 627, 203
Heggie D. C., 1975, MNRAS, 173, 729
M. H{\'e}non,1975, International Astronomical Union. Symposium,69,133.
Hills J. G., Day C. A., 1976, Astrophys. Lett., 17, 87
Hobbs G., Lorimer D. R., Lyne A. G., Kramer M., 2005, MNRAS, 360, 974
Hurley J. R., Tout C. A., Pols O. R., 2002, MNRAS, 329, 897
Jordán A. et al., 2007, ApJS, 171, 101
Kimball C., Talbot C., Berry C. P. L., Carney M., Zevin M., Thrane E., Kalogera V., 2020, ApJ, 900, 177
Kimball C. et al., 2021, ApJ, 915, L35

Kremer K. et al., 2020, ApJ, 903, 45
Kroupa P., 2001, MNRAS, 322, 231
Kulkarni S. R., Hut P., McMillan S. J., 1993, Nature, 364, 421
Liu B., Lai D., 2021, MNRAS, 502, 2049
Madau P., Dickinson M., 2014, ARA&A, 52, 415
Mandel I., De Mink S. E., 2016, MNRAS, 458, 2634
Mapelli M., Bouffanais Y., Santoliquido F., Arca Sedda M., Artale M. C., 2022, MNRAS, 511, 5797
Miller M. C., Lauburg V. M., 2009, ApJ, 692, 917
Mink S. E. d., Belczynski K., 2015, ApJ, 814, 58
Mould M. , Gerosa D. , Taylor S. R. , 2022, PhRvD, 106, 103013
O'Leary R. M., Kocsis B., Loeb A., 2009, MNRAS, 395, 2127
Olejak A. , Fryer C. L. , Belczynski K. , Baibhav V. , 2022, MNRAS, 516, 2252
Park D., Kim C., Lee H. M., Bae Y.-B., Belczynski K., 2017, MNRAS, 469, 4665
Peters P., 1964, Phys. Rev., 136, B1224
Portegies Zwart S. F., McMillan S. L. W., 2000, ApJ, 528, L17
Portegies Zwart S., Gaburov E., Chen H.-C., Gürkan M. A., 2007, MNRAS, 378, L29
Rezzolla L., Barausse E., Dorband E. N., Pollney D., Reisswig C., Seiler J., Husa S., 2008, Phys. Rev. D, 78, 044002
Rodriguez C. L., Morscher M., Pattabiraman B., Chatterjee S., Haster C.-J., Rasio F. A., 2015, Phys. Rev. Lett., 115, 051101
Rodriguez C. L., Chatterjee S., Rasio F. A., 2016, Phys. Rev. D, 93, 084029
Rodriguez C. L., Amaro-Seoane P., Chatterjee S., Rasio F. A., 2018, Phys. Rev. Lett., 120, 151101
Rodriguez C. L. et al., 2020, ApJ, 896, L10
Romero-Shaw I. M. , Lasky P. D. , Thrane E. , 2022, ApJ, 940, 171
Salpeter E. E., 1955, ApJ, 121, 161
Samsing J., 2018, Phys. Rev. D, 97, 103014
Sigurdsson S., Hernquist L., 1993, Nature, 364, 423
Silsbee K., Tremaine S., 2017, ApJ, 836, 39
Spera M., Mapelli M., 2017, MNRAS, 470, 4739
Stegmann J. , Antonini F. , Schneider F. R. N. , Tiwari V. , Chattopadhyay D. , 2022, PhRvD, 106, 023014
Stone N. C., Metzger B. D., Haiman Z., 2016
Tagawa H., Haiman Z., Bartos I., Kocsis B., Omukai K., 2021a, MNRAS, 507, 3362
Tagawa H., Kocsis B., Haiman Z., Bartos I., Omukai K., Samsing J., 2021b, ApJ, 908, 194
Tiwari V., Fairhurst S., 2021, ApJ, 913, L19
van Son L. A. C. et al., 2022, ApJ, 940, 184
VandenBerg D. A., Brogaard K., Leaman R., Casagrande L., 2013, ApJ, 775, 134
Vink J. S., de Koter A., 2005, A&A, 442, 587
Vink J. S., de Koter A., Lamers H. J. G. L. M., 2001, A&A, 369, 574
Woosley S. E., 2017, ApJ, 836, 244
Yang Y. et al., 2019, Phys. Rev. Lett., 123, 181101
Zevin M. , Holz D. E. , 2022, ApJ, 935, 20

APPENDIX A:

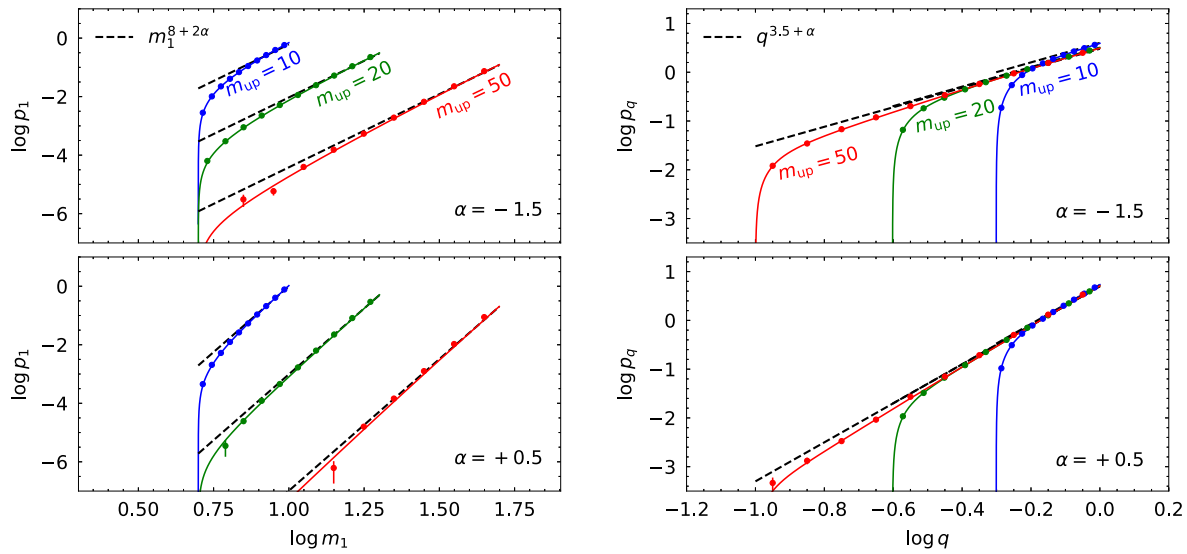

Figure A1. PDFs for m_1 (left) and q (right) for different BH mass function upper masses (m_{up}) and logarithmic slopes (α). In all cases $m_{lo} = 5$. The results discussed in the text [equations (B4) and (B6)] are shown as full lines, whereas the dots with errors bars show Monte Carlo realizations (as a check) obtained by drawing 10^6 pairs from p_I (m_I) [equation (B3)] and the black dashed lines show simple power-law approximations.

APPENDIX B: MASS SAMPLING ROUTINES

B1 Masses of three-body binaries

We are interested in the probability density functions (PDFs) of the masses of the two components of (BH) binaries that form in three-body interactions. Following Heggie (1975), the formation rate of hard binaries per unit of volume and energy is expressed as

$$\Gamma_{3b}(m_{\rm I}, m_{\rm II}, m_{\rm III}, x) = n_{\rm I} n_{\rm II} n_{\rm III} Q(m_{\rm I}, m_{\rm II}, m_{\rm III}, x), \tag{B1}$$

where $n_i = n(m_i)$ is the number density of BHs with mass m_i, $m_{\rm I}$ and $m_{\rm II}$ are the masses of the stars ending up in the binary, $m_{\rm III}$ is the mass of the catalyst star and x is the (positive) binding energy of the binary. The rate function Q is given by equation 4.14 in Heggie (1975) and it is a function of the three masses, as well as their $\beta_i = (m_i \sigma_i^2)^{-1}$, where σ_i is the one-dimensional velocity dispersion of mass component i. Because binaries tend to form from the most massive objects, for which energy equipartition is established quickly, we assume $\beta_{\rm I} = \beta_{\rm II} = \beta_{\rm III} = \beta$. Integrating equation 4.14 from Heggie over all x, from the hard-soft boundary (i.e. $x = \beta^{-1}$) to ∞ (i.e. all hard binaries), we find that the formation rate of hard binaries per unit of volume is

$$\Gamma_{3b}(m_{\rm I}, m_{\rm II}, m_{\rm III}) \propto n_{\rm I} n_{\rm II} n_{\rm III} \frac{(m_{\rm I} m_{\rm II})^4 m_{\rm III}^{5/2}}{\sqrt{(m_{\rm I}+m_{\rm II}+m_{\rm III})(m_{\rm I}+m_{\rm II})}} \beta^{9/2}. \tag{B2}$$

For equal masses, this result reduces to the frequently used scaling $\Gamma_{3b}(m) \propto n^3 m^5 \sigma^{-9}$. Equation (B2) is symmetric in $m_{\rm I}$ and $m_{\rm II}$, so the PDF for the mass of one of them is found from

$$p_{\rm I}(m_{\rm I}) = \int_{m_{\rm lo}}^{m_{\rm up}} \int_{m_{\rm lo}}^{m_{\rm up}} {\rm d}m_{\rm III} {\rm d}m_{\rm II}\, \Gamma_{3b}, \tag{B3}$$

and $p_{\rm II}(m_{\rm II}) = p_{\rm I}(m_{\rm I})$. Here, $m_{\rm lo}$ and $m_{\rm up}$ are the lower and upper bound of the mass distribution, respectively.

We note here that equation (B2) includes the assumption of equipartition and therefore takes into account the dependence of the velocity dispersion on mass. On the other hand, we do not consider the change in the BH mass function that is expected in the core due to mass segregation. Numerical simulations have shown that the mass function in the core has a logarithmic slope that is approximately only +1 steeper than the global mass function (e.g. Portegies Zwart et al. 2007). Thus, we expect the effect of mass segregation on our results to be relatively small.

We now adopt the convention that m_1 and m_2 are the most massive and least massive component, respectively, with corresponding PDFs $p_1(m_1)$ and $p_2(m_2)$. These correspond to the PDFs of the maximum and minimum value, respectively, when a sample of two values are drawn from $p_{\rm I}(m_{\rm I})$, and are given by

$$p_1(m_1) = 2 P_{\rm I}(m_1) p_{\rm I}(m_1), \tag{B4}$$

$$p_2(m_2) = 2 [1 - P_{\rm I}(m_2)]\, p_{\rm I}(m_2), \tag{B5}$$

where $P_I(m_I) = \int_{m_{\rm lo}}^{m_I} {\rm d}m'_I\, p_I(m'_I)$ is the cumulative density function of $p_{\rm I}(m_{\rm I})$.

The PDF of q is a ratio distribution and can be found from the joint distribution of the minimum and maximum values, which is given by $p_{12}(m_1, m_2) = 2\, p_1(m_1)\, p_2(m_2)$ and

$$p_q(q) = \int_{m_{\rm lo}}^{m_{\rm up}} {\rm d}m_2\, p_{12}(q m_2, m_2). \tag{B6}$$

We then assume that the mass function is a power law such that $n_i \propto m_i^{\alpha}$ between $m_{\rm lo}$ and $m_{\rm up}$. A value of $\alpha = 0.5$ provides a good approximation of the mass function of BHs at low metallicities ($Z \lesssim 0.05\, Z_\odot$, see fig. 4 of Antonini & Gieles 2020b). In Fig. A1, we show the resulting $p_1(m_1)$ and $p_q(q)$ for $m_{\rm up} = [10, 20, 50]$ and $m_{\rm lo} = 5$ and $\alpha = +0.5$ (approximate for metal-poor GCs) and $\alpha = -1.5$ (approximate for metal-rich GCs). We find that these PDFs can be reasonably well approximated by power-laws of the form: $p_1(m_1) \propto m_1^{8+2\alpha}$ and $p_q(q) \propto q^{3.5+\alpha}$, for all values of $m_{\rm up}$ and α. This approximation can be used to sample m_1 and m_2 (via q).

B2 Masses of interlopers

Assume a binary BH with mass $M_{12} = m_1 + m_2$, moving in a field of BHs with number density n_3. The rate of encounters between the BH binaries and field BHs is (Hills & Day 1976)

$$\dot{N}_3 = n_3 \langle \Sigma v \rangle, \tag{B7}$$

where v is the relative velocity between the binary BH and another BH and Σ is the cross-section for an encounter, which in the gravitational focusing regime is (Hills & Day 1976)

$$\Sigma \simeq \frac{2\pi G a M_{123}}{v^2}, \tag{B8}$$

where G is the gravitational constant, $M_{123} = M_{12} + m_3$ and a is the semimajor axis of the binary. We can find $\langle \Sigma v \rangle$ from integrating over all velocities

$$\langle \Sigma v \rangle = \frac{4 l^3}{\pi^{1/2}} \int_0^{\infty} \Sigma(v) v^3 \exp(-l^2 v^2) {\rm d}v, \tag{B9}$$

$$= 4\pi^{1/2} G l M_{123} a. \tag{B10}$$

Here, $l^2 = \beta\, M_{12}\, m_3/(2 M_{123})$ for our assumption of equipartition. The semimajor axis is $a \propto Gm_1\, m_2 \beta$ such that the interaction rate scales with the masses as

$$\dot{N}_3 \propto m_3^{\alpha} \sqrt{m_3} \sqrt{M_{12} M_{123}} m_1 m_2 \tag{B11}$$

So, interactions with more massive BHs are slightly favoured wrt random draws from the BH mass function. Because $p_1(m_1)$ and $p_2(m_2)$ are much steeper than this distribution, we find that to good approximation $p_3(m_3) \propto m_3^{\alpha+1/2}$. It also means that exchanges are not very important, because these happen when the intruder is more massive than any of the binary members. Here, we find for $m_{\rm up}/m_{\rm lo} = 10$ and $\alpha = +0.5$ that $\langle m_1 \rangle \simeq 0.91\, m_{\rm up}$; $\langle m_2 \rangle \simeq 0.76\, m_{\rm up}$ and $\langle m_3 \rangle \simeq 0.55\, m_{\rm up}$ and exchange interactions should therefore not be very common. Once the width of the BH mass function has shrunk to $m_{\rm up}/m_{\rm lo} \simeq 2$, $\langle m_2 \rangle \simeq 0.78$, which is comparable with $\langle m_3 \rangle \simeq 0.75$ and exchange interactions (which we neglect) are more relevant.

This paper has been typeset from a TEX/LATEX file prepared by the author.